LETTER

doi:10.1038/nature09568

Entanglement of spin waves among four quantum memories

K. S. Choi[1], A. Goban[1], S. B. Papp[1]†, S. J. van Enk[2] & H. J. Kimble[1]

Quantum networks are composed of quantum nodes that interact coherently through quantum channels, and open a broad frontier of scientific opportunities[1]. For example, a quantum network can serve as a 'web' for connecting quantum processors for computation[2,3] and communication[4], or as a 'simulator' allowing investigations of quantum critical phenomena arising from interactions among the nodes mediated by the channels[5,6]. The physical realization of quantum networks generically requires dynamical systems capable of generating and storing entangled states among multiple quantum memories, and efficiently transferring stored entanglement into quantum channels for distribution across the network. Although such capabilities have been demonstrated for diverse bipartite systems[7–12], entangled states have not been achieved for interconnects capable of 'mapping' multipartite entanglement stored in quantum memories to quantum channels. Here we demonstrate measurement-induced entanglement stored in four atomic memories; user-controlled, coherent transfer of the atomic entanglement to four photonic channels; and characterization of the full quadripartite entanglement using quantum uncertainty relations[13–16]. Our work therefore constitutes an advance in the distribution of multipartite entanglement across quantum networks. We also show that our entanglement verification method is suitable for studying the entanglement order of condensed-matter systems in thermal equilibrium[17,18].

Diverse applications in quantum information science require coherent control of the generation, storage and transfer of entanglement among spatially separated physical systems[1–6]. Despite its inherently multipartite nature, entanglement has been studied primarily for bipartite systems[3], where remarkable progress has been made in harnessing physical processes to generate 'push-button' and 'heralded' entanglement[7–10,19,20], as well as to map entangled states to and from atoms, photons and phonons[11,12].

For multipartite systems, the 'size' of a physical state, described by the system's density matrix, $\hat{\rho}_N$, grows exponentially with the number of subsystems, N, and makes the entangled states exceedingly difficult to represent with classical information. Importantly, this complexity of $\hat{\rho}_N$ increases the potential utility of multipartite entanglement in quantum information science, including quantum algorithms[2,3] and simulation[5]. Redundant encoding of quantum information into multipartite entangled states allows quantum error correction and fault-tolerant computation[2,3]. Intricate long-range correlation of many-body systems is intimately intertwined with the behaviour of multipartite entanglement[17,18]. In addition, mobilizing multipartite entanglement across quantum networks could lead to novel quantum phase transitions for the network[6].

Counterposed to these opportunities, the complex structure of multipartite entanglement presents serious challenges both for its formal characterization and physical realization[3,18,21,22]. Indeed, there are relatively few examples of laboratory systems that have successfully generated multipartite entanglement[15,23–27]. Most works have considered the entanglement in spin systems, notably trapped ions[23,24], which are applicable to the matter nodes of quantum networks. But the methodologies for verifying multipartite entanglement are problematic for infinite-dimensional bosonic systems of the quantum channels (for example multipartite quadrature[25,26] and number-state[15] entanglement for optical modes). A-posteriori multipartite entanglement has been inferred from a small subset of preferred photon detection events from parametric down-conversion[27].

In addition to the characterization of multipartite entanglement, an important capability of quantum networks is provided by quantum interfaces capable of generating, storing and dynamically allocating the entanglement of matter nodes into photonic channels (see ref. 28 and references therein). Here we introduce such a quantum interface for quadripartite entangled states based upon coherent, collective emission from matter to light, as illustrated in Fig. 1a. We present a systematic study of the generation and storage of quadripartite entangled states of spin waves in a set of four nodes of atomic memories, as well as of the coherent transfer of the entangled components of the material state into individual photonic channels. We observe transitions of M-partite to $(M-1)$-partite entangled states via controlled spin-wave statistics of the atomic memories, as well as the dynamic evolution of multipartite entanglement in a dissipative environment, from fully quadripartite entangled states to unentangled states.

Our experiment proceeds in four steps (Methods). First, in step (i), an entangled state, $\hat{\rho}_{\mathrm{W}}^{(\mathrm{A})}$, of four atomic ensembles is generated by quantum interference in a quantum measurement[4,7] (Fig. 1b). Given a photoelectric detection event at detector $\mathrm{D_h}$, the conditional atomic state is ideally a quadripartite entangled state, $\hat{\rho}_{\mathrm{W}}^{(\mathrm{A})} = |W\rangle_{\mathrm{A}}\langle W|$, with

$$|W\rangle_{\mathrm{A}} = \frac{1}{2}\left[\left(|\bar{s}_a,\bar{g}_b,\bar{g}_c,\bar{g}_d\rangle + \mathrm{e}^{i\phi_1}|\bar{g}_a,\bar{s}_b,\bar{g}_c,\bar{g}_d\rangle\right) + \mathrm{e}^{i\phi_2}\left(|\bar{g}_a,\bar{g}_b,\bar{s}_c,\bar{g}_d\rangle + \mathrm{e}^{i\phi_3}|\bar{g}_a,\bar{g}_b,\bar{g}_c,\bar{s}_d\rangle\right)\right] \quad (1)$$

whose single quantum spin wave, $|\bar{s}_\varepsilon\rangle$, is coherently shared among four ensembles, $\varepsilon \in \{a,b,c,d\}$. These entangled states are known as W states, and comprise atomic ground states, $|\bar{g}_\varepsilon\rangle = |g\cdots g\rangle_\varepsilon$, and single collective excitations, $|\bar{s}_\varepsilon\rangle = (1/\sqrt{N_{\mathrm{A},\varepsilon}})\sum_{i=1}^{N_{\mathrm{A},\varepsilon}}|g\cdots s_i\cdots g\rangle_\varepsilon$, where $N_{\mathrm{A},\varepsilon}$ is the number of atoms in ensemble ε.

After the heralding event, step (ii) consists of storage of $\hat{\rho}_{\mathrm{W}}^{(\mathrm{A})}$ in the ensembles for a user-controlled time, τ. At the end of this interval, step (iii) is initiated with read beams to coherently transfer the entangled atomic components of $\hat{\rho}_{\mathrm{W}}^{(\mathrm{A})}$ into a quadripartite entangled state of light, $\hat{\rho}_{\mathrm{W}}^{(\gamma)} = |W\rangle_\gamma\langle W|$, by means of cooperative emissions[4] (Fig. 1c), where

$$|W\rangle_\gamma = \frac{1}{2}\left[\left(|1000\rangle + \mathrm{e}^{i\phi'_1}|0100\rangle\right) + \mathrm{e}^{i\phi'_2}\left(|0010\rangle + \mathrm{e}^{i\phi'_3}|0001\rangle\right)\right] \quad (2)$$

This photonic state is a mode-entangled W state[15,16], which shares a single delocalized photon among four spatially separated optical modes, $\gamma_2 \in \{a_2,b_2,c_2,d_2\}$.

Finally, in step (iv) we characterize the heralded entanglement for $\hat{\rho}_{\mathrm{W}}^{(\gamma)}$ from complementary measurements of photon statistics and

[1]Norman Bridge Laboratory of Physics 12-33, California Institute of Technology, Pasadena, California 91125, USA. [2]Department of Physics, University of Oregon, Eugene, Oregon 97403, USA. †Present address: National Institute of Standards and Technology, Boulder, Colorado 80305, USA.

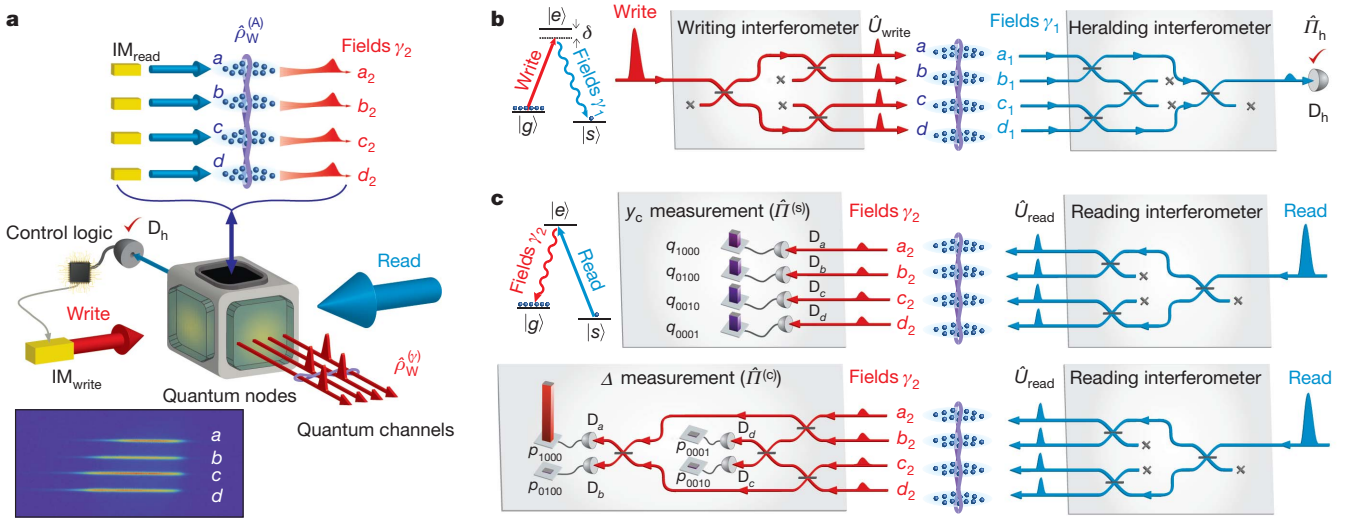

Figure 1 | Overview of the experiment. **a**, Quantum interfaces for multipartite quantum networks. Inset, a fluorescence image of the laser-cooled atomic ensembles *a*, *b*, *c* and *d* that become entangled (Methods). IM_{read} and IM_{write} are the respective intensity modulators of the read and write lasers. **b**, Entanglement generation. A weak write laser (red-detuned by $\delta = 10$ MHz from the $|g\rangle \rightarrow |e\rangle$ transition) is split into four components to excite the atomic ensembles by means of parametric interactions, $\hat{U}_{write}$, leading to Raman scattered fields, $\gamma_1 \in \{a_1, b_1, c_1, d_1\}$, emitted by the ensembles. The entangled state, $\hat{\rho}_W^{(A)}$, for four atomic ensembles $\varepsilon \in \{a,b,c,d\}$ (equation (1)) is heralded by a projective measurement, $\hat{\Pi}_h$, at detector D_h, derived from quantum interference of four fields γ_1 in the heralding interferometer. **c**, Quantum state exchange and entanglement verification. Read lasers are applied to the ensembles to transform the atomic entangled state $\hat{\rho}_W^{(A)}$ coherently into quadripartite entangled beams of light, $\hat{\rho}_W^{(\gamma)}$ (equation (2)) by means of quantum state transfers, $\hat{U}_{read}$, with each beam propagating through quantum channels $\gamma_2 \in \{a_2, b_2, c_2, d_2\}$. Subpanel for y_c measurement: the quantum statistics, q_{ijkl}, for the individual modes of $\hat{\rho}_W^{(\gamma)}$ with $i, j, k, l \in \{0, 1\}$ photons are measured with projectors $\hat{\Pi}_i^{(s)}$ at detectors D_a, D_b, D_c, D_d. Subpanel for Δ measurement: mutual coherences for $\hat{\rho}_W^{(A)}$ are accessed with projectors $\hat{\Pi}_i^{(c)}$ from detection statistics p_{ijkl} at D_a, D_b, D_c, D_d. Further details are given in Supplementary Information.

coherence[15,16] (Fig. 1c). In particular, we consider a reduced density matrix, $\hat{\rho}_r = p_0\hat{\rho}_0 + p_1\hat{\rho}_1 + p_{\geq 2}\hat{\rho}_{\geq 2}$, containing up to one photon per mode, which leads to a lower bound for the entanglement of the actual physical states, $\hat{\rho}_W^{(A)}$ and $\hat{\rho}_W^{(\gamma)}$. Here p_0, p_1 and $p_{\geq 2}$ are the probabilities of the zero- and one-photon subspaces ($\hat{\rho}_0$ and $\hat{\rho}_1$) and the higher-order subspaces ($\hat{\rho}_{\geq 2}$), which can be populated for any realistic system. As illustrated in the upper panel of Fig. 1c, we characterize the statistical contamination of $\hat{\rho}_W^{(\gamma)}$ due to $\hat{\rho}_0$ and $\hat{\rho}_{\geq 2}$ with a normalized measure[16]—namely $y_c \equiv (8/3)p_{\geq 2}p_0/p_1^2$, which ranges from $y_c = 0$, for a single excitation, to $y_c = 1$, for balanced coherent states—by detecting the photon statistics, q_{ijkl}, of γ_2 at the output faces of the ensembles.

We also quantify the mutual coherences of $\hat{\rho}_W^{(\gamma)}$ by measuring the photon probabilities p_{1000}, p_{0100}, p_{0010} and p_{0001} at the outputs of the verification (v) interferometer. We determine the sum uncertainty, $\Delta \equiv \sum_{i=1}^{N=4} \left\langle \left(\hat{\Pi}_i^{(c)}\right)^2 - \left\langle \hat{\Pi}_i^{(c)} \right\rangle^2 \right\rangle$ for the variables $\hat{\Pi}_i^{(c)} = |W_i\rangle_v\langle W_i|$, which project $\hat{\rho}_r$ onto a set of four orthonormal W states, $|W_i\rangle_v$, with phases, $\beta_i \in \{\beta_1, \beta_2, \beta_3\}_v$, selected by the actively stabilized paths in the verification interferometer (Supplementary Information). Hence, for the ideal W state (equation (2)) with $\beta_i = \phi' i$, we have $\Delta = 0$ associated with $p_{1000} = 1$ and $p_{0100} = p_{0010} = p_{0001} = 0$, as observed in the bar plots of the lower panel of Fig. 1c for $y_c = 0.04 \pm 0.01$. In contrast, mixed states with no phase coherences would result in balanced probabilities ($p_{1000} = p_{0100} = p_{0010} = p_{0001} = 1/4$) and $\Delta = 0.75$.

The pair $\{\Delta, y_c\}$ thereby defines the parameter space for the multipartite entanglement in our experiment, with the entanglement parameters Δ and y_c serving as a non-local, nonlinear entanglement witness[16]. Our criterion for 'genuine' M-partite entanglement takes the most stringent form of non-separability (ref. 22 and references therein) and excludes all weaker forms of entanglement (Methods). Specifically, for a given value of y_c, we determine the boundary, $\Delta_b^{(M-1)}$, for the minimal uncertainty possible for all states containing at most $(M-1)$-mode entanglement and their mixtures (Supplementary Information). For our quadripartite states ($N = 4$), we derive $\Delta_b^{(3)}$, $\Delta_b^{(2)}$ and $\Delta_b^{(1)}$ for tripartite entangled, bipartite entangled and fully separable states, respectively, as functions of y_c. Thus, a measurement of quantum statistics (y_c) and the associated coherence (Δ) with $\Delta < \Delta_b^{(3)}, \Delta_b^{(2)}, \Delta_b^{(1)}$ manifestly confirms the presence of genuine ($M = 4$)-partite entanglement[15,16]. Furthermore, we can unambiguously distinguish genuine M-partite and $(M-1)$-partite entangled states for any $M \leq N$ by observing Δ below $\Delta_b^{(M-1)}$.

Figure 2 presents our results for quadripartite entanglement for a storage time of $\tau_0 = 0.2$ μs. We first investigate off-diagonal coherence for the purportedly entangled atomic and photonic states, $\hat{\rho}_W^{(A)}$ and $\hat{\rho}_W^{(\gamma)}$, in Fig. 2a. As the bipartite phase, β_2, is varied, we observe interferences in p_{1000}, p_{0100}, p_{0010} and p_{0001}, and, hence, a variation in Δ that results from the coherence between the bipartite entangled components of $\hat{\rho}_W^{(\gamma)}$ for the modes $\{a_2, b_2\}$ and $\{c_2, d_2\}$. Furthermore, for optimal settings of β_2, the observed values of Δ (Fig. 2a, black points) fall below the bounds $\Delta_b^{(3)}$, $\Delta_b^{(2)}$ and $\Delta_b^{(1)}$ (red, green and purple bands, respectively) for $y_c = 0.06 \pm 0.02$, and signal the generation of a fully quadripartite entangled state. The observed quadripartite entanglement arises from the intrinsic indistinguishability of probability amplitudes for one collective excitation, $|\bar{s}_\varepsilon\rangle$, among the four ensembles. We also present results from a control experiment with a 'crossed' state, $\hat{\rho}_\times^{(A)}$ (Fig. 2a, orange points), that consists of an incoherent mixture of entangled pairs $\{a, b\}$ and $\{c, d\}$ (Methods).

Next we characterize $\hat{\rho}_W^{(\gamma)}$ (and $\hat{\rho}_W^{(A)}$) over the full parameter space, $\{\Delta, y_c\}$. In a regime of weak excitation (with excitation probability $\xi \ll 1$) for the ensemble–field pairs $\{\varepsilon, \gamma_1\}$, the heralded state $\hat{\rho}_W^{(A)}$ is approximately

$$\hat{\rho}_W^{(A)}(\tau = 0) \approx (1 - 3\xi)|W\rangle_A\langle W| + 3\xi\hat{\rho}_{\geq 2}^{(A)} + \mathcal{O}(\xi^2) \qquad (3)$$

where $\hat{\rho}_{\geq 2}^{(A)}$ includes uncorrelated spin waves with two or more quanta in the set of four ensembles due to atomic noise. As $\xi \rightarrow 0$, a heralding event at D_h leads to a state with high fidelity to $|W\rangle_A$ stored in the four ensembles. However, for increasing ξ, $\hat{\rho}_{\geq 2}^{(A)}$ becomes important, leading to modifications of the spin-wave statistics for $\hat{\rho}_W^{(A)}$ and, thereby, to the entanglement parameters $\{\Delta, y_c\}$. Hence, by varying ξ through the

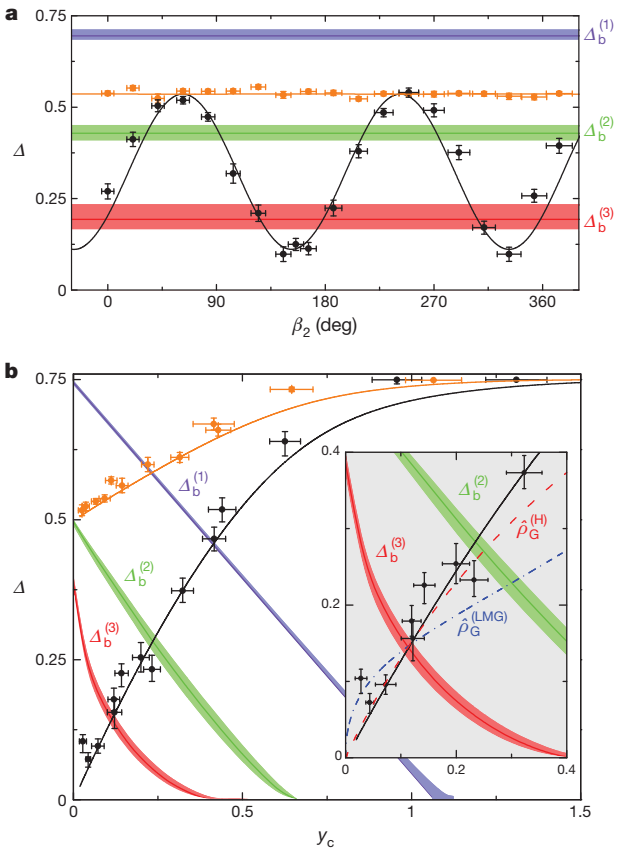

Figure 2 | Quadripartite entanglement among four atomic ensembles. **a**, Quantum interference between the bipartite entangled pairs of the full quadripartite state (black points) as a function of bipartite phase β_2. **b**, Exploring the entanglement space $\{\Delta, y_c\}$ for quadripartite states. By controlling the spin-wave statistics, we observe transitions from quadripartite entangled states to tripartite entangled, bipartite entangled and fully separable states (black points). We also display our results for the 'crossed' quantum state, $\hat{\rho}_\times^{(A)}$ (orange points), as further described in Methods. Inset, expanded view of entanglement parameters $\{\Delta, y_c\}$. Results for entanglement thermalization, characterized by $\Delta^{(T)}$ and $y_c^{(T)}$, of the spin systems $\hat{\rho}_G^{(H)}$ and $\hat{\rho}_G^{(LMG)}$ are shown by the red dashed and blue dash–dot lines, respectively. The red, green and purple bands respectively represent the minimum uncertainties for three-mode ($\Delta_b^{(3)}$) and two-mode entanglement ($\Delta_b^{(2)}$), and for fully separable states ($\Delta_b^{(1)}$); the thickness of each band from the central line corresponds to ± 1 s.d. of the corresponding bound. In all cases, error bars for the data reflect the statistical and systematic uncertainties (Supplementary Information).

overall intensity for the write beam, we adjust the quantum statistics (y_c) and coherence (Δ) of the entangled states $\hat{\rho}_W^{(A)}$ and $\hat{\rho}_W^{(\gamma)}$.

This procedure is used in Fig. 2b to parametrically increase Δ and y_c in tandem. As y_c is increased from $y_c \approx 0$ in the quantum domain to $y_c \approx 1$ in the classical regime, we observe transitions of the directly measured photonic states $\hat{\rho}_W^{(\gamma)}$ (Fig. 2b, black points) from fully quadripartite entangled states ($\Delta < \Delta_b^{(3)}$) to tripartite entangled ($\Delta_b^{(3)} < \Delta < \Delta_b^{(2)}$), to bipartite entangled ($\Delta_b^{(2)} < \Delta < \Delta_b^{(1)}$) and, finally, to fully separable states ($\Delta_b^{(1)} < \Delta$). As shown by the curves, our observations correspond well to a theoretical model of the entanglement parameters, $\{\Delta^{th}, y_c^{th}\}$, for entanglement generation, transfer and verification (Supplementary Information). In comparison with our former work on the coherent splitting of a photon[15], the heralded atomic and photonic W states, $\hat{\rho}_W^{(A)}$ and $\hat{\rho}_W^{(\gamma)}$, offer qualitatively richer statistical passages through the entanglement spaces delineated by Δ and y_c. Here the quantum coherence (Δ) is intrinsically linked to the statistical character (y_c) owing to quantum correlations between the heralding fields, γ_1, and the excitation statistics of the ensembles.

For $\xi \ll 1$, the coherent contribution, $\hat{\rho}_c^{(A)}$, of the delocalized single quantum strongly dominates any other processes for the full quadripartite state, $\hat{\rho}_W^{(A)}$, in equation (3). With a heralding probability $p_h \approx 3 \times 10^{-4}$ ($\xi \approx 5 \times 10^{-3}$), we achieve the smallest entanglement parameters, $\Delta^{min} = 0.07^{+0.01}_{-0.02}$ and $y_c^{min} = 0.038 \pm 0.006$, for the generated quadripartite entangled states. These parameters are suppressed below the closest three-mode boundary $\Delta_b^{(3)}$ by ten standard deviations (Supplementary Information). Furthermore, because the local mapping of quantum states from matter to light cannot increase entanglement[7], our measurements of $\hat{\rho}_W^{(\gamma)}$ unambiguously provide a lower bound of the quadripartite entanglement stored in $\hat{\rho}_W^{(A)}$. Therefore, the observed strong violation of the uncertainty relations for Δ^{min} and y_c^{min} categorically certifies the creation of measurement-induced entanglement of spin waves among four quantum memories, as well as the coherent transfer of the stored quadripartite entangled states to an entangled state of four propagating electromagnetic fields.

In terms of state fidelity, our approach to the generation of heralded multipartite entanglement compares favourably to matter systems using local interactions (for example trapped ions[23,24]). Despite the intrinsically low preparation probability, the resulting quadripartite entangled state, $\hat{\rho}_W^{(A)}$, stored in the four ensembles has high fidelity with the ideal W state, namely $F^{(A)} = {}_A\langle W|\hat{\rho}_W^{(A)}|W\rangle_A$. As discussed in Methods, we estimate a lower bound for the unconditional entanglement fidelity of $F^{(A)} \geq 0.9 \pm 0.1$, to be compared with the theoretical fidelity, $F_{th}^{(A)} = 0.98$, derived for the parameters in our experiment.

Apart from the creation of novel multipartite entangled spin waves, an important benchmark of a quantum interface is the transfer efficiency, λ, of multipartite entanglement from matter to light[11]. Because no known measure applies to our case, we tentatively define the entanglement transfer $\lambda = F^{(\gamma)}/F^{(A)}$, with physical fidelity $F^{(\gamma)} = {}_\gamma\langle W|\hat{\rho}_W^{(\gamma)}|W\rangle_\gamma$ for the photonic state $\hat{\rho}_W^{(\gamma)}$. In particular, for $\xi \ll 1$ we obtain $F_{th}^{(\gamma)} \approx \eta_{read} F_{th}^{(A)}$, which gives $\lambda_{th} \approx \eta_{read} = 38 \pm 4\%$, dictated by the retrieval efficiency, η_{read}. Although fidelity is an often used measure, we emphasize that $F^{(\gamma)}$ cannot be used to set a threshold for entanglement, because $\hat{\rho}_W^{(\gamma)}$ can exhibit multipartite entanglement for any $F^{(\gamma)} > 0$.

To investigate the dynamical behaviour of the observed quadripartite entangled states, we study the temporal evolution of multipartite entanglement stored in the atomic ensembles as a function of a storage time, τ. Decoherence for the atomic W state is governed by motional dephasing of spin waves[29], in which the imprinted atomic phases in $|\bar{s}_\varepsilon\rangle$ evolve independently owing to thermal motion, thereby transforming the initial collective state into a subradiant state uncorrelated with the heralding fields, γ_1 (Supplementary Information). The net effect is an increase of both entanglement parameters, $\{\Delta, y_c\}$, with a timescale $\tau_m \approx 17$ μs (Methods). Eventually, the growth in $\Delta(\tau)$ and $y_c(\tau)$ leads to time-dependent losses of entanglement, marked by successive crossings of the boundaries set by $\Delta_b^{(3)}$, $\Delta_b^{(2)}$ and $\Delta_b^{(1)}$.

In Fig. 3a, we examine the dissipative dynamics of multipartite entanglement for the quantum memories of four ensembles through the evolution of both Δ and y_c. We observe the passage of the initial quadripartite entangled state, $\hat{\rho}_W^{(A)}(\tau_0)$ at $\tau_0 = 0.2$ μs, through various domains, progressively evolving from M-partite entanglement to $(M-1)$-partite entanglement at memory times $\tau = \tau_m^{(M-1)}$, with the final state, $\hat{\rho}_W^{(A)}(\tau_f)$, measured at $\tau_f = 36.2$ μs. The crossings of the bounds $\Delta_b^{(3)}$, $\Delta_b^{(2)}$ and $\Delta_b^{(1)}$ occur at $\tau_m^{(3)} = 15$ μs, $\tau_m^{(2)} = 21$ μs and $\tau_m^{(1)} = 24$ μs, respectively. In addition, the measured entanglement parameters evolve in qualitative agreement with the simulated dynamics derived for $\hat{\rho}_W^{(A)}(\tau)$ from our theoretical model (solid line), with deviations (especially for Δ^{th}) discussed in Supplementary Information. Figure 3b shows the parametric losses of entanglement in terms of $\Delta(\tau)$ and $y_c(\tau)$.

Finally, an interesting extension is to relate the characterization of multipartite entanglement by means of $\{\Delta, y_c\}$ to the relaxations of entanglement in quantum many-body systems[17,18]. We consider two

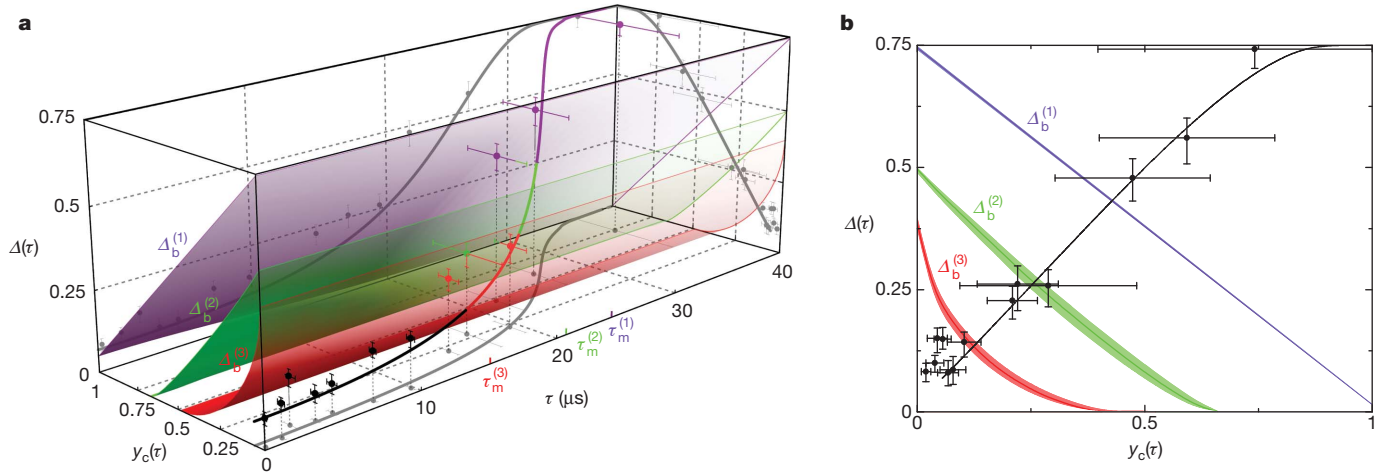

Figure 3 | Dissipative dynamics of atomic entanglement. **a**, Dynamic evolution of entanglement parameters $\Delta(\tau)$ and $y_c(\tau)$ for the multipartite quantum state. We observe crossing of the boundaries defined by three-mode (red surface, $\Delta_b^{(3)}$) and two-mode (green surface, $\Delta_b^{(2)}$) entangled states, and separable states (purple surface, $\Delta_b^{(1)}$). We indicate various entanglement orders for quadripartite (black), tripartite (red) and bipartite entangled (green) states, and fully separable states (purple) for the data points and the curve. The projections of the data points onto the y_c–τ and Δ–τ planes show the individual passages of $\Delta(\tau)$ and $y_c(\tau)$ (Supplementary Information and Supplementary Movie 1). **b**, Projection of entanglement dynamics onto the Δ–y_c plane. The curves in **a** and **b** are from a theoretical model including motional dephasing. Error bars for the data represent the statistical and systematic uncertainties.

ferromagnetic spin models (Heisenberg-like and Lipkin–Meshkov–Glick Hamiltonians $\hat{H}_H$ and, respectively, $\hat{H}_{LMG}$) as well as their thermal entanglement, as characterized by $\{\Delta^{(T)}, y_c^{(T)}\}$ (Supplementary Information). Results of our analysis for the Gibbs thermal equilibrium states $\hat{\rho}_G^{(H)}$ of $\hat{H}_H$ and $\hat{\rho}_G^{(LMG)}$ of $\hat{H}_{LMG}$ are shown by the red dashed and, respectively, blue dash–dot lines in the inset of Fig. 2b. The statistical character of $\hat{\rho}_W^{(A)}$ for our system of four ensembles follows the thermalization of $\hat{\rho}_G^{(H)}$ and $\hat{\rho}_G^{(LMG)}$ for $y_c \lesssim 0.2$, whereby $\hat{\rho}_{\geq 2}^{(A)}$ is thermally populated. This comparison suggests that our method of entanglement characterization could be applied to access the link between off-diagonal long-range order and multipartite entangled spin waves in thermalized quantum magnets[17,18].

In conclusion, our measurements explicitly demonstrate a coherent matter–light quantum interface for multipartite entanglement by way of the operational metric of quantum uncertainty relations[14–16]. High-fidelity, entangled spin waves are generated in four spatially separated atomic ensembles and coherently transferred to quadripartite entangled beams of light. The quantum memories are individually addressable and can be readily read out at different times for conditional control of entanglement[4]. With recent advances by other groups, the short memory times obtained in Fig. 3 could be improved beyond 1 s (Methods).

Further possibilities include the creation of yet larger multipartite entangled states with efficient scaling[4] for the realization of multipartite quantum networks. For example, quadripartite entangled states of ensemble sets $\{a, b, c, d\}$ and $\{a', b', c', d'\}$ could be extended by swapping between a and a' to prepare a hexapartite entangled state for $\{b, b', c, c', d, d'\}$ (Methods). Generalization of such processes will allow the preparation of a single macroscopic entangled state for observing entanglement percolation[6] and extreme non-locality of W states[30], as well as for studying quantum phase transitions in strongly correlated systems[17,18]. Finally, the entangled spin waves can be applied to quantum metrology to detect a phase shift of π in an unknown component of $\hat{\rho}_W^{(A)}$ with efficiency beyond any separable state (Methods).

METHODS SUMMARY

The preparation stage of our quantum interface lasts $\Delta t_p = 22$ ms, and consists of laser-cooling and trapping a large cloud of caesium atoms in a magneto-optical trap, from which the atoms are further laser-cooled in an optical molasses and prepared in the state $|g\rangle$ on release from the trap. We define the four cold atomic ensembles with well-separated optical paths of the quantum fields γ_1 and γ_2, which are individually addressed by laser pulses. To operate the quantum interface, we apply a sequence of writing and repumping pulses to the atomic ensembles with a repetition rate of 2 MHz over $\Delta t_q = 3$ ms, followed by the next preparation stage. Detection of a spontaneously scattered Raman photon, γ_1, at D_h triggers a control logic, which terminates the writing and repumping lasers, leaving the ensembles without optical illumination and inhomogeneous broadening, for the quantum storage of heralded multipartite entanglement. The resulting local production rate for the atomic quadripartite entanglement with parameters Δ^{min} and y_c^{min} during Δt_q is $r_q \approx 500$ Hz, giving an average rate of $r_p \approx 60$ Hz. After a storage time τ, read pulses individually transfer the entangled atomic components to propagating multipartite entangled fields, γ_2, via superradiant emissions. In Methods, we describe our spin-wave quantum memories (Fig. 1a, inset) and a control experiment on a 'crossed' quantum state, $\hat{\rho}_\times^{(A)}$, that results from the intrinsic distinguishability of two bipartite components, as shown in Fig. 2a. We also derive expressions for entanglement fidelity and for the relationship between the set of mutual coherences $d_{\alpha\beta}$ (between modes $\alpha, \beta \in \{a_2, b_2, c_2, d_2\}$) and Δ. In addition, we discuss the prospects for improving our experiment. Finally, we present a quantum-enhanced parameter estimation protocol for using entangled spin waves to detect an atomic phase shift of π with efficiency beyond the limit set by separable states.

Full Methods and any associated references are available in the online version of the paper at www.nature.com/nature.

Received 4 July; accepted 5 October 2010.

1. Kimble, H. J. The quantum internet. *Nature* **453,** 1023–1030 (2008).
2. Preskill, J. Quantum computation. *Phys. 219 Course Inf.* ⟨http://www.theory.caltech.edu/people/preskill/ph219/#lecture⟩ (1997).
3. Nielsen, M. A. & Chuang, I. L. *Quantum Computation and Quantum Information* (Cambridge Univ. Press, 2000).
4. Duan, L.-M., Lukin, M. D., Cirac, J. I. & Zoller, P. Long-distance quantum communication with atomic ensembles and linear optics. *Nature* **414,** 413–418 (2001).
5. Lloyd, S. Universal quantum simulator. *Science* **273,** 1073–1078 (1996).
6. Acín, A., Cirac, J. I. & Lewenstein, M. Entanglement percolation in quantum networks. *Nature Phys.* **3,** 256–259 (2007).
7. Chou, C. W. *et al.* Measurement-induced entanglement for excitation stored in remote atomic ensembles. *Nature* **438,** 828–832 (2005).
8. Moehring, D. L. *et al.* Entanglement of single-atom quantum bits at a distance. *Nature* **449,** 68–71 (2007).
9. Simon, J., Tanji, H., Ghosh, S. & Vuletić, V. Single-photon bus connecting spin-wave quantum memories. *Nature Phys.* **3,** 765–769 (2007).
10. Weber, B. *et al.* Photon-photon entanglement with a single trapped atom. *Phys. Rev. Lett.* **102,** 030501 (2009).
11. Choi, K. S., Deng, H., Laurat, J. & Kimble, H. J. Mapping photonic entanglement into and out of a quantum memory. *Nature* **452,** 67–71 (2008).
12. Jost, J. D. *et al.* Entangled mechanical oscillators. *Nature* **459,** 683–685 (2009).
13. Sørensen, A. & Mølmer, K. Entanglement and extreme spin squeezing. *Phys. Rev. Lett.* **86,** 4431–4434 (2001).
14. Hofmann, H. F. & Takeuchi, S. Violation of local uncertainty relations as a signature of entanglement. *Phys. Rev. A* **68,** 032103 (2003).
15. Papp, S. B. *et al.* Characterization of multipartite entanglement for one photon shared among four optical modes. *Science* **324,** 764–768 (2009).

16. Lougovski, P. *et al.* Verifying multipartite mode entanglement of *W* states. *N. J. Phys.* **11,** 063029 (2009).
17. Amico, L., Fazio, R., Osterloh, A. & Vedral, V. Entanglement in many-body systems. *Rev. Mod. Phys.* **80,** 517–576 (2008).
18. Gühne, O. & Tóth, G. Entanglement detection. *Phys. Rep.* **474,** 1–75 (2009).
19. Steffen, M. *et al.* Measurement of the entanglement of two superconducting qubits via state tomography. *Science* **313,** 1423–1425 (2006).
20. DiCarlo, L. *et al.* Demonstration of two-qubit algorithms with a superconducting quantum processor. *Nature* **460,** 240–244 (2009).
21. van Enk, S. J., Lütkenhaus, N. & Kimble, H. J. Experimental procedures for entanglement verification. *Phys. Rev. A* **75,** 052318 (2007).
22. Horodecki, R., Horodecki, P., Horodecki, M. & Horodecki, K. Quantum entanglement. *Rev. Mod. Phys.* **81,** 865–942 (2009).
23. Leibfried, D. *et al.* Creation of a six-atom 'Schrödinger cat' state. *Nature* **438,** 639–642 (2005).
24. Haffner, H. *et al.* Scalable multiparticle entanglement of trapped ions. *Nature* **438,** 643–646 (2005).
25. Aoki, T. *et al.* Experimental creation of a fully inseparable tripartite continuous-variable state. *Phys. Rev. Lett.* **91,** 080404 (2003).
26. Su, X. *et al.* Experimental preparation of quadripartite cluster and Greenberger-Horne-Zeilinger entangled states for continuous variables. *Phys. Rev. Lett.* **98,** 070502 (2007).
27. Gao, W.-B. *et al.* Experimental demonstration of a hyper-entangled ten-qubit Schrödinger cat state. *Nature Phys.* **6,** 331–335 (2010).
28. Lvovsky, A. I., Sanders, B. C. & Tittel, W. Optical quantum memory. *Nature Photon.* **3,** 706–714 (2009).
29. Simon, J. & Tanji, H. Thompson, J. K. & Vuletić, V. Interfacing collective atomic excitations and single photons. *Phys. Rev. Lett.* **98,** 183601 (2007).
30. Heaney, L., Cabello, A., Santos, M. F. & Vedral, V. Extreme nonlocality with one photon. Preprint at ⟨http://arxiv.org/abs/0911.0770v2⟩ (2010).

Supplementary Information is linked to the online version of the paper at www.nature.com/nature.

Acknowledgements We acknowledge discussions with K. Hammerer, P. Zoller and J. Ye. This research is supported by the National Science Foundation, the DOD NSSEFF program, the Northrop Grumman Corporation and the Intelligence Advanced Research Projects Activity. A.G. acknowledges support by the Nakajima Foundation. S.B.P. acknowledges support received as a fellow of the Center for Physics of Information at Caltech.

Author Contributions All authors contributed extensively to the research presented in this paper.

Author Information Reprints and permissions information is available at www.nature.com/reprints. The authors declare no competing financial interests. Readers are welcome to comment on the online version of this article at www.nature.com/nature. Correspondence and requests for materials should be addressed to H.J.K. (hjkimble@caltech.edu).

METHODS

Experimental details. The experiment consists of a 22-ms preparation stage and a 3-ms period for operating the quantum interface in Fig. 1 with a repetition rate of 40 Hz and a duty cycle of $D_c = 3/25$. For the preparation stage, we load and laser-cool caesium atoms (peak optical depth, ~30) in a magneto-optical trap for 18 ms, after which the atoms are released from the trap with dynamically compensated eddy currents. The atoms are further cooled in an optical molasses ($T_t \approx 150$ μK) for 3.8 ms and optically pumped to $|g\rangle$ for 0.2 ms. During this time, a phase reference laser ($F = 3 \leftrightarrow F' = 4$ transition) also propagates through the atomic ensembles for the active stabilization of the verification interferometer in Fig. 1c by means of *ex situ* phase modulation spectroscopy[15], which does not affect the operation of the quantum interface (Supplementary Information). Concurrently, dense caesium atoms in paraffin-coated vapour cells located at the heralding and verification ports are prepared in the ground states $|g\rangle$ and $|s\rangle$ for filtering the coherent-state lasers scattered into the respective quantum fields, γ_1 and γ_2.

Quantum interface. For the quantum interface to function during the 3-ms window, in step (i) 20-ns writing pulses (red-detuned by $\delta = 10$ MHz from the $|g\rangle \rightarrow |e\rangle$ transition) and 100-ns repumping pulses (resonant with $|s\rangle \rightarrow |e\rangle$) are applied sequentially to the ensembles ε, synchronized to a clock running at $R_c \approx 2$ MHz. This process creates pairwise correlated excitations[4] between the collective atomic modes, $|\bar{s}_\varepsilon\rangle$, of the ensembles ε and the optical fields γ_1 ($\delta = 10$ MHz below $|e\rangle \rightarrow |s\rangle$). Photodetection of a single photon for the combined fields γ_1 at the output of the heralding interferometer effectively erases the 'which-path' information for γ_1, and imprints the entangled spin wave $\hat{\rho}_W^{(A)}$ (equation (3)) onto the ensembles a, b, c and d via $\mathrm{Tr}_h\left(\hat{\Pi}_h \hat{U}_{write}^{\dagger} \hat{\rho}_g^{(A)} \hat{U}_{write}\right)$. The heralding event at D_h triggers control logic (Fig. 1a) that deactivates intensity modulators of the writing (IM_{write}), repumping and reading lasers (IM_{read}) for the quantum storage of $\hat{\rho}_W^{(A)}$ in step (ii). After a user-controlled delay, τ, step (iii) is initiated with 20-ns, strong read pulses (Rabi frequency of 24 MHz, resonant with $|s\rangle \rightarrow |e\rangle$) that address the ensembles in Fig. 1c and coherently transfer the entangled atomic components a, b, c and d of $\hat{\rho}_W^{(A)}(\tau)$ one by one to propagating beams $\gamma_2 \in \{a_2, b_2, c_2, d_2\}$ (resonant with $|e\rangle \rightarrow |g\rangle$), comprising the entangled photonic state $\hat{\rho}_W^{(\gamma)}(\tau)$, via the operation $\hat{\rho}_W^{(\gamma)} = \mathrm{Tr}_A\left(\hat{U}_{read}^{\dagger} \hat{\rho}_W^{(A)} \hat{U}_{read}\right)$. Here Tr_A traces over the atomic systems that are later shelved into the ground states $|\bar{g}_\varepsilon\rangle$. The retrieval efficiency, η_{read}, is collectively enhanced for large N_A (ref. 4), leading to $\eta_{read} = 0.38 \pm 0.06$ in our experiment. The average production rate for the atomic quadripartite entanglement for $\{\Delta^{min}, y_c^{min}\}$ is $r_p = R_c D_c p_h \approx 60$ Hz, and the actual rate during the 3-ms operating window is $r_q = R_c p_h \approx 500$ Hz. The atomic level diagrams for entanglement generation and quantum state exchanges are shown as insets to Fig. 1b, c. States $|g\rangle$ and $|s\rangle$ are the hyperfine ground states $F = 4$ and $F = 3$ of $6S_{1/2}$ in atomic caesium, respectively; state $|e\rangle$ is the hyperfine level $F' = 4$ of the electronic excited state $6P_{3/2}$.

Spin-wave quantum memories. The quantum information of the entangled state for equation (1) is encoded in the quantum numbers of spin waves (collective excitations) for the pseudo-spin of the hyperfine ground electronic levels $6S_{1/2}$ ($F = 3$, $F = 4$) in atomic caesium. The fluorescence images shown in the inset of Fig. 1a depict the collective atomic modes of ensembles $\varepsilon \in \{a, b, c, d\}$ for exciting the entangled spin waves $\hat{\rho}_W^{(A)}$ with 1-mm separations and 60-μm waists. The geometry of the collective excitations for the four ensembles a, b, c and d is defined by the point-spread functions of the imaging systems for the fields γ_1 and γ_2, where each ensemble consists of a cold cloud of $N_{A,\varepsilon} \approx 10^6$ caesium atoms. We use an off-axial configuration[31] to address each ensemble ε individually, with an angle of $\theta = 2.5^\circ$ between the classical and non-classical beams (Supplementary Information), that creates spin waves $|\bar{s}_\varepsilon\rangle$ associated with wavevectors $\delta\mathbf{k} = \mathbf{k}_{write} - \mathbf{k}_{\gamma_1}$ for each ε. These spin waves are analogous to other types of collective excitation in many-body systems, such as magnons and plasmons, and can be converted to dark-state polaritons for the coherent transfer, $\hat{U}_{read}$, of entanglement. For the phase-matching configuration and temperature of our ensembles, the memory times $\tau_m^{(3)}$, $\tau_m^{(2)}$ and $\tau_m^{(1)}$ (Fig. 3) are dominantly determined by the motional dephasing of the spin waves $|\bar{s}_\varepsilon\rangle$ (ref. 29). For a thermal velocity of $v_t \approx 14$ cm s^{-1}, we estimate a memory time of $\tau_m \approx (0.85\ \mu\mathrm{m})/4\pi \sin(\theta/2) v_t = 17$ μs. However, the ground-state dephasing due to inhomogeneous broadening is expected to be >50 μs in our experiment, as inferred from two-photon Raman spectroscopy.

Quantum uncertainty relations and genuine multipartite entanglement. To verify the entanglement by way of Δ and y_c, we first evaluate the photon statistics p_0, p_1 and $p_{\geq 2}$ for the measurement of y_c. Operationally, this is accomplished by measuring the individual probabilities, q_{ijkl}, for $i, j, k, l \in \{0, 1\}$ photons to occupy the respective optical modes $\gamma_2 \in \{a_2, b_2, c_2, d_2\}$ at the output faces of the ensembles, through photoelectric detections $\hat{\Pi}_i^{(s)}$. For the measurement of Δ, we quantify the off-diagonal coherence, $\bar{d}$, of $\hat{\rho}_W^{(\gamma)}$ by pairwise interferences of all possible sets of modes α, $\beta \in \{a_2, b_2, c_2, d_2\}$ with the verification interferometer. The photon probabilities p_{1000}, p_{0100}, p_{0010} and p_{0001} at the output modes of the verification interferometer thereby result from the coherent interferences of the four purportedly entangled fields γ_2 that depend on the phase orientations $\{\beta_1, \beta_2, \beta_3\}_v$ of $\hat{\Pi}_i^{(c)}$ (Supplementary Information).

Our conclusion of genuine multipartite entanglement for the atomic and photonic states $\{\hat{\rho}_W^{(A)}, \hat{\rho}_W^{(\gamma)}\}$ does not rely on weaker conditions based on the non-separability along any fixed bipartition of $\{\hat{\rho}_W^{(A)}, \hat{\rho}_W^{(\gamma)}\}$. The genuine M-partite entangled states created from our experiment can only be represented as mixtures of pure states that all possess M-partite entanglement, as for the case of genuine 'k-producibility' in multipartite spin models[17,18]. We note that our entanglement verification protocol cannot be used to verify the absence of entanglement for the physical state $\hat{\rho}_W^{(\gamma)}$ in an infinite dimension[32]. Finally, we emphasize that our analysis makes use of the full physical state, $\{\hat{\rho}_W^{(A)}, \hat{\rho}_W^{(\gamma)}\}$, including the vacuum component, $\hat{\rho}_0$, and higher-order terms, $\hat{\rho}_{\geq 2}$, and does not rely upon a spurious postdiction based on a preferred set of detection events (Supplementary Information).

Generation and characterization of a 'crossed' quantum state. As a control experiment, we reconfigure the heralding interferometer such that path information could in principle be revealed up to the bipartite split of the ensemble pairs $\{a, b\}$ and $\{c, d\}$ by analysing the polarization state of the heralding photon, γ_1. In this case, the heralding measurement, $\hat{\Pi}_\times$, prepares a 'crossed' atomic state, $\hat{\rho}_\times^{(A)}$, with no coherence shared between $\{a, b\}$ and $\{c, d\}$. Thus, we observe an absence of interference in Fig. 2a (orange points). However, this modified $\hat{\Pi}_\times$ preserves the bipartite entanglement within $\{a, b\}$ and $\{c, d\}$, which explains our observation of the uncertainty, Δ, reduced below the one-mode bound, $\Delta_b^{(1)}$, for $y_c = 0.07 \pm 0.01$. Similarly, we also detect the statistical transition from bipartite entanglement to fully separable states for the 'crossed' state in Fig. 2b, despite the disentanglement for the bipartition (|) of $\{a, b\}|\{c, d\}$.

Relationship between quantum uncertainty and off-diagonal coherences. Here we derive the general expression for the upper bound of the sum uncertainty, Δ, as a function of the coherence, $\bar{d}$. First we note that Δ is only sensitive to the one-excitation subspace, $\hat{\rho}_1$, of $\hat{\rho}_r$

$$\hat{\rho}_1 = \begin{pmatrix} s_{1000} & d_{ab} & d_{ac} & d_{ad} \\ d_{ba}^* & s_{0100} & d_{bc} & d_{bd} \\ d_{ca}^* & d_{cb}^* & s_{0010} & d_{cd} \\ d_{da}^* & d_{db}^* & d_{dc}^* & s_{0001} \end{pmatrix}$$

normalized such that $\mathrm{Tr}(\hat{\rho}_1) = s_{1000} + s_{0100} + s_{0010} + s_{0001} = 1$. Here the diagonal elements, $\mathbf{s}_1 = (s_{1000}, s_{0100}, s_{0010}, s_{0001})$, of $\hat{\rho}_1$ are related to the one-photon probabilities, $\mathbf{q}_1 = (q_{1000}, q_{0100}, q_{0010}, q_{0001})$, at the faces of the ensembles by $p_1 \mathbf{s}_1 = \mathbf{q}_1$. By transforming $\hat{\rho}_1$ into the basis spanned by $|W_i\rangle_v$, we then find the expressions for the normalized output photon probabilities, p_{1000}, p_{0100}, p_{0010} and p_{0001}, of the verification interferometer as functions of $\mathbf{s}_1$ and $d_{\alpha\beta}$. The sum uncertainty, Δ, is then expressed as

$$\Delta = \frac{3}{4} - \left\{ \left(|d_{ab}| + |d_{cd}|\right)^2 + \left(|d_{ac}| + |d_{bd}|\right)^2 + \left(|d_{ad}| + |d_{bc}|\right)^2 \right\}$$

Thus, we obtain $\Delta \lesssim (3/4)(1 - 16\bar{d}^2)$. The average value of the six unique off-diagonal elements is $\bar{d} = (1/6)\sum_{\alpha,\beta} |d_{\alpha\beta}|$ with $0 \leq \bar{d} \leq 1/4$, and the effective interference visibility is given by $V_{eff} = 4\bar{d}$.

Derivation of entanglement fidelity. Here we obtain the expression for the lower-bound unconditional entanglement fidelity, $F^{(A)} = \tilde{p}_1 F_1$, where $\tilde{p}_1$ is the probability of a single spin wave, $\hat{\rho}_1^{(A)}$, in the heralded state $\hat{\rho}_W^{(A)}$ and $F_1 = \langle W_1 | \hat{\rho}_1^{(A)} | W_1 \rangle$ is the conditional fidelity for $\hat{\rho}_1^{(A)}$. We start by noting that the projective measurement $\hat{\Pi}_i^{(c)}$ for Δ gives the conditional fidelity, F_1, of $\hat{\rho}_r$ projected onto one of four orthonormal W states, $|W_i\rangle_v = |W_1\rangle_v$, for example $|1000\rangle + e^{i\beta_1}|0100\rangle + e^{i\beta_2}\left(|0010\rangle + e^{i\beta_3}|0001\rangle\right)$. Hence, we can define $\Delta = 1 - F_1^2 - \sum_{i=2}^4 F_i^2$ in terms of the respective overlaps F_i. Because of the orthonormality condition, $\sum_{i=1}^4 F_i = 1$, the sum uncertainty is bounded by $\Delta \geq 1 - F_1^2 - (1 - F_1)^2$, from which we obtain $F_1 \geq \sqrt{(1/2)(1/2 - \Delta)} + 1/2$. Finally, by multiplying a factor of $\tilde{p}_1$, the probability of exciting one spin wave distributed among the four ensembles, we find the lower-bound fidelity $F^{(A)} \geq \tilde{p}_1\left(\sqrt{(1/2)(1/2 - \Delta)} + 1/2\right)$ obtained unconditionally for the heralded atomic state $\hat{\rho}_W^{(A)}$. In principle, the imbalances in the interferometer can rotate the projectors into non-orthonormal sets[16]. However, the measured losses and the beam-splitter ratios are well-enough balanced that any changes in $F^{(A)}$ due to modified projectors are well within the uncertainties of the data, as evidenced by the close-to-unity projection fidelity, $F^{(\pi)} = 99.9^{+0.1}_{-0.2}\%$ (Supplementary Information). In the experiment, $\tilde{p}_1$ and F_1 are determined from the inferences of the spin-wave statistics (by means of y_c) and the coherences (by means of Δ), respectively.

Prospects for improving memory time and matter–light transfer efficiency. By operating the clock speed at $R_c \rightarrow 10$ MHz and $\tau_m^{(3)} \approx 20$ μs, we could prepare hexapartite ($M = 6$) entanglement with probability $3z\eta_{read}p_h^2/8 \approx 10^{-5}$ by connecting two quadripartite states $\hat{\rho}_W^{(A)}$ for Δ^{min} and y_c^{min}, with enhancement

factor $z = 400$ (ref. 33), thereby giving a local production rate of $r_q \approx 50$–100 Hz, or an average rate of $r_p \approx 5$–10 Hz with our current duty cycle, D_c. The most challenging aspect of verifying the hexapartite entangled states is the quantification of the higher-order contamination, $\hat{\rho}_{\geq 2}$, which we estimate to be one event per 10 h. This integration rate is feasible with our current system. More generally, M_1-partite and M_2-partite entangled states can be fused by entanglement connection to create an $M = (M_1 + M_2 - 2)$-partite entangled state. However, the memory times $\tau_m^{(3)}$, $\tau_m^{(2)}$ and $\tau_m^{(1)}$ (Fig. 3) and the entanglement transfer, λ, from matter to light limit our ability to scale the multipartite entanglement beyond $M > 6$ by way of conditional control and connection of entanglement[33,34] with our current experimental parameters.

The prerequisite storage techniques for suppressing both the internal and the motional spin-wave dephasings can be extended for τ_m with advances in ensemble-based quantum memories[35,36,37]). Recent experiments with single ensembles have achieved coherence times of up to $\tau_m \approx 1.5$ s in quantum degenerate gases[38,39], albeit with efficiencies of $\lesssim 1\%$. Also, the transfer efficiency can be increased to $\lambda_{th} \approx 0.9$ by enclosing the ensembles within high-finesse cavities[29]. System integrations by way of atom-chip technology and waveguide coupling[40,41] hold great potential for scalability given the strong cooperativity and the long coherence[42]. At this level, two or more heralded processes of multipartite entanglement generation can be made on-demand on timescales of $\tau_{det} \approx 1/R_c p_h = 1$ ms, with $\tau_m \gg \tau_{det}$ (refs 33, 34).

Realistically, the expansion of multipartite entangled states $\hat{\rho}_W^{(A)}$ will be limited by the intrinsic degradations of the entanglement parameters Δ and y_c, which inevitably increase with each step of entanglement connection[34], and by the specific quantum repeater architecture implemented on $\hat{\rho}_W^{(A)}$. The latter is an extremely rich area of research in view of the large classes of methods for connecting multipartite entangled states, making it premature to specify a particular architecture for multipartite entanglement expansion. However, our experiment will hopefully stimulate theoretical studies of complex repeater architectures for multipartite systems, beyond traditional one-to-one networks[43].

Quantum-enhanced parameter estimation with entangled spin waves. We describe a quantum-enhanced parameter estimation protocol whereby a phase shift in a single ensemble, ε_i, of the quadripartite state $\varepsilon_i \in \{a, b, c, d\}$ can be detected with efficiency beyond that for any separable state. Specifically, we consider a π phase shift, $\hat{U}_{\pi,\varepsilon_i} = \exp(i\pi\hat{n}_{\varepsilon_i})$, applied to an unknown spin-wave component $\varepsilon_i \in \{a, b, c, d\}$ ($\hat{n}_{\varepsilon_i} = \hat{S}_{\varepsilon_i}^{\dagger}\hat{S}_{\varepsilon_i}$) of the atomic state $\hat{\rho}_W^{(A)}$, or to a spatial field mode, $\gamma_{2i} \in \{a_2, b_2, c_2, d_2\}$, of the photonic state $\hat{\rho}_W^{(\gamma)}$ ($\hat{n}_{\gamma_{2i}} = \hat{a}_{\gamma_{2i}}^{\dagger}\hat{a}_{\gamma_{2i}}$). Our goal is to find the π-phase-shifted ensemble, ε_i (or optical mode, γ_{2i}), in a single measurement under the condition that an average of one spin wave is populated in total; that is, $\sum_i \mathrm{Tr}\left(\hat{n}_{\varepsilon_i}\hat{\rho}_W^{(A)}\right) = 1$ (or, for optical modes, $\sum_i \mathrm{Tr}\left(\hat{n}_{\gamma_{2i}}\hat{\rho}_W^{(\gamma)}\right) = 1$). As a quantum benchmark, we consider an average success probability $P_s = (1/4)\sum_{\varepsilon_i} \mathrm{Tr}\left(\hat{\Pi}_{\varepsilon_i}^{(u)}\hat{U}_{\pi,\varepsilon_i}^{\dagger}\hat{\rho}_W^{(A)}\hat{U}_{\pi,\varepsilon_i}\right)$ (failure probability, $P_f = 1 - P_s$) for distinguishing the phase-shifted ensemble ε_i (or mode γ_{2i}) among the four possibilities $\varepsilon_i \in \{a, b, c, d\}$ (or $\gamma_{2i} \in \{a_2, b_2, c_2, d_2\}$) by way of unambiguous quantum state discrimination, $\hat{\Pi}_{\varepsilon_i}^{(u)}$ (refs 44–47).

First we consider an ideal W state, $|W\rangle_o = |W\rangle_A$ (or $|W\rangle_{\gamma_2}$), with atomic phases $\phi_i \in \{\phi_1, \phi_2, \phi_3\}$ (or photonic phases $\phi'_i \in \{\phi'_1, \phi'_2, \phi'_3\}$). In this case, the π-phase-shifted entangled W states $|W_{\varepsilon_i}\rangle_f \in \left\{\left|W_a^{(\pi)}\right\rangle_f, \left|W_b^{(\pi)}\right\rangle_f, \left|W_c^{(\pi)}\right\rangle_f, \left|W_d^{(\pi)}\right\rangle_f\right\}$ can be detected deterministically, because $\left|W_{\varepsilon_i}^{(\pi)}\right\rangle_f = \hat{U}_{\pi,\varepsilon_i}|W\rangle_o$ forms an orthonormal complete set that spans the state space of $\hat{\rho}_1$, resulting from the underlying symmetry of $|W\rangle_o$ with respect to any rotation $\hat{U}_{\pi,\varepsilon_i}$ on a generalized Bloch sphere. Operationally, we set the verification phases $\beta_{1,2} - \phi'_{1,2} = 0$ and $\beta_3 - \phi'_3 = \pi$. Then the π-phase-shifted ensemble, ε_i, can be unambiguously distinguished because the otherwise balanced output photon probabilities, $\mathbf{p}_v = (p_{1000}, p_{0100}, p_{0010}, p_{0001}) = (0.25, 0.25, 0.25, 0.25)$, of the verification interferometer will be transformed to $\mathbf{p}_v = (1,0,0,0)$, for a π phase induced in ensemble a, to $\mathbf{p}_v = (0,1,0,0)$ in ensemble b, to $\mathbf{p}_v = (0,0,1,0)$ in ensemble c and to $\mathbf{p}_v = (0,0,0,1)$ in ensemble d, each with success probability $P_s^{(ent)} = 1$.

For fully separable states $|\Psi\rangle_o = |\psi_a\rangle_a|\psi_b\rangle_b|\psi_c\rangle_c|\psi_d\rangle_d$, with $|\psi_{\varepsilon_i}\rangle_{\varepsilon_i} = \sum_{n=0}^{\infty} c_{\varepsilon_i}^{(n)}|n\rangle_{\varepsilon_i}$, we displace the resulting π-phase-shifted state, $\left|\Psi_{\varepsilon_i}^{(\pi)}\right\rangle_f = \hat{U}_{\pi,\varepsilon_i}|\Psi\rangle_o$, with a local unitary transformation, $\hat{V}_{\varepsilon_i}|\psi_{\varepsilon_i}\rangle_{\varepsilon_i} = |0\rangle_{\varepsilon_i}$. The overall process, $\hat{V}_a\hat{V}_b\hat{V}_c\hat{V}_d\hat{U}_{\pi,\varepsilon_i}$, maps the initial product state, $|\Psi\rangle_o$, into $\hat{V}_a\hat{U}_{\pi,a}|\psi_a\rangle_a|0\rangle_b|0\rangle_c|0\rangle_d$ (phase shift in ensemble a), $|0\rangle_a\hat{V}_b\hat{U}_{\pi,b}|\psi_b\rangle_b|0\rangle_c|0\rangle_d$ (ensemble b), $|0\rangle_a|0\rangle_b\hat{V}_c\hat{U}_{\pi,c}|\psi_c\rangle_c|0\rangle_d$ (ensemble c) or $|0\rangle_a|0\rangle_b|0\rangle_c\hat{V}_d\hat{U}_{\pi,d}|\psi_d\rangle_d$ (ensemble d), with only one ε_i containing $\langle\hat{n}_{\varepsilon_i}\rangle > 0$ excitations. Thus, we can unambiguously identify the phase-shifted ensemble given a photodetection, albeit with a failure probability

$$P_f = \frac{1}{4}\sum_{\varepsilon_i}\left|{}_{\varepsilon_i}\langle 0|\hat{V}_{\varepsilon_i}\hat{U}_{\pi,\varepsilon_i}|\psi_{\varepsilon_i}\rangle_{\varepsilon_i}\right|^2 = \frac{1}{4}\sum_{\varepsilon_i}\left|{}_{\varepsilon_i}\langle\psi_{\varepsilon_i}|\hat{U}_{\pi,\varepsilon_i}|\psi_{\varepsilon_i}\rangle_{\varepsilon_i}\right|^2$$

arising from inconclusive null events (that is, $|0000\rangle\langle 0000|$). We derive the maximum success probability, $P_s^{(max)} = 1 - P_f^{(min)}$, and the optimal state, $|\Psi\rangle_o = |\Psi\rangle_{opt}$, by minimizing $P_f^{(min)}$ over all possible realizations of $c_{\varepsilon_i}^{(n)}$ satisfying $\sum_{\varepsilon_i}\langle\psi_{\varepsilon_i}|\hat{n}_{\varepsilon_i}|\psi_{\varepsilon_i}\rangle_{\varepsilon_i} = 1$. Specifically, we find that an optimal (pure) separable state $|\Psi\rangle_{opt} = \Pi_{\varepsilon_i}\left(\sqrt{3/4}|0\rangle_{\varepsilon_i} + \sqrt{1/4}|1\rangle_{\varepsilon_i}\right)$ can be used for the parameter estimation protocol to infer ε_i with $P_s^{(max)} = 0.75$. Similarly, the maximum success probability $P_s^{(coh)}$ can be derived for multimode coherent states $\Pi_{\varepsilon_i}|\alpha_{\varepsilon_i}\rangle_{\varepsilon_i}$, giving a classical bound of $P_s^{(coh)} = 1 - 1/e$.

Finally, we consider the upper bound $P_s^{(max)}$ for mixed separable states, $\hat{\rho}_o^{(sep)}$, with pure state decompositions $\hat{\rho}_o^{(sep)} = \sum_m p_m|\Psi_m\rangle_o\langle\Psi_m|$. Generally, the transformations $\hat{V}_{\varepsilon_i}$, as discussed above, do not exist for $\hat{\rho}_o^{(sep)}$, precluding the possibility of unambiguous state discrimination. Thus, the success probability, $P_s\left(\hat{\rho}_o^{(sep)}\right)$, is bounded from above by the convex combinations of $|\Psi_m\rangle$, such that

$$P_s\left(\hat{\rho}_o^{(sep)}\right) \leq \sum_m p_m P_s\left(|\Psi_m\rangle_o\langle\Psi_m|\right) \leq P_s^{(max)} = 0.75$$

Importantly, the maximum success probability, $P_s^{(max)} = 0.75$, attainable for any $\hat{\rho}_o^{(sep)}$, is less than $P_s^{(ent)} = 1$ for entangled states $|W\rangle_o$. Thus, the entangled spin waves in the experiment can be used to sense an atomic phase shift beyond the limit for any unentangled state. A comprehensive analysis of our protocol, including experimental imperfections (for example detection efficiency) and other measurement strategies, will be discussed elsewhere.

31. Balić, V., Braje, D. A., Kolchin, P., Yin, G. Y. & Harris, S. E. Generation of paired photons with controllable waveforms. *Phys. Rev. Lett.* **94,** 183601 (2005).
32. Eisert, J., Simon, C. & Plenio, M. B. On the quantification of entanglement in infinite-dimensional quantum systems. *J. Phys. A* **35,** 3911–3923 (2002).
33. Chou, C.-W. *et al.* Functional quantum nodes for entanglement distribution over scalable quantum networks. *Science* **316,** 1316–1320 (2007).
34. Laurat, J. *et al.* Towards experimental entanglement connection with atomic ensembles in the single excitation regime. *N. J. Phys.* **9,** 207–220 (2007).
35. Hammerer, K., Sorensen, A. S. & Polzik, E. S. Quantum interface between light and atomic ensembles. *Rev. Mod. Phys.* **82,** 1041–1093 (2010).
36. Zhao, R. *et al.* Long-lived quantum memory. *Nature Phys.* **5,** 100–104 (2009).
37. Zhao, B. *et al.* A millisecond quantum memory for scalable quantum networks. *Nature Phys.* **5,** 95–99 (2009).
38. Schnorrberger, U. *et al.* Electromagnetically induced transparency and light storage in an atomic Mott insulator. *Phys. Rev. Lett.* **103,** 033003 (2009).
39. Zhang, R., Garner, S. R. & Hau, L. V. Creation of long-term coherent optical memory via controlled nonlinear interactions in Bose-Einstein condensates. *Phys. Rev. Lett.* **103,** 233602 (2009).
40. Colombe, Y. *et al.* Strong atom-field coupling for Bose–Einstein condensates in an optical cavity on a chip. *Nature* **450,** 272–276 (2007).
41. Vetsch, E. *et al.* Optical interface created by laser-cooled atoms trapped in the evanescent field surrounding an optical nanofiber. *Phys. Rev. Lett.* **104,** 203603 (2010).
42. Deutsch, C. *et al.* Spin self-rephasing and very long coherence times in a trapped atomic ensemble. *Phys. Rev. Lett.* **105,** 020401 (2010).
43. Sangouard, N., Simon, C., de Riedmatten, H. & Gisin, N. Quantum repeaters based on atomic ensembles and linear optics. Preprint at ⟨http://arxiv.org/abs/0906.2699v2⟩ (2009).
44. Ivanovic, I. D. How to differentiate between non-orthogonal states. *Phys. Lett. A* **123,** 257–259 (1987).
45. Dieks, D. Overlap and distinguishability of quantum states. *Phys. Lett. A* **126,** 303–306 (1988).
46. Peres, A. How to differentiate between non-orthogonal states. *Phys. Lett. A* **128,** 19 (1988).
47. Chefles, A. Unambiguous discrimination between linearly independent quantum states. *Phys. Lett. A* **239,** 339–347 (1998).